



Atmospheric erosion and replenishment induced by impacts upon the Earth and Mars during a heavy bombardment

D. de Niem^{a,*}, E. Kührt^a, A. Morbidelli^b, U. Motschmann^{a,c}

^aDLR Institute of Planetary Research, Rutherford Str. 2, D-12489 Berlin, Germany

^bObservatoire de la Côte d'Azur, CNRS, BP 4229, 06304 Nice Cedex 4, France

^cInstitute of Theoretical Physics, Technical University of Braunschweig, Mendelssohnstrasse 3, D-38106 Braunschweig, Germany

ARTICLE INFO

Article history:

Received 9 November 2011

Revised 23 July 2012

Accepted 23 July 2012

Available online 22 August 2012

Keywords:

Atmospheres, Evolution

Cratering

Earth

Impact processes

Mars

ABSTRACT

Consequences of a heavy bombardment for the atmospheres of Earth and Mars are investigated with a stochastic model. The main result is the dominance of the accumulation. The atmospheric pressure is strongly increasing both for Earth and Mars in the course of an enhanced bombardment. The effect of atmospheric erosion is found to be minor, regarding escape during meteorite entry, in the expanding vapor plume, and ejection due to free-surface motion. The initial atmospheric surface pressure if comparable to the modern value turns out as a less important additive constant of the final pressure. Impactor retention and atmospheric erosion are parametrized in terms of scaling laws, compatible with recent numerical simulations. The dependence on impactor size, atmospheric and planetary parameters is analyzed among alternative models and numerical results. The stochastic model is fed with the net replenishment originating from impactor material and the loss of preexisting atmospheric gas. Major input parameters are the total cumulative impactor mass and the relative mass of atmophile molecules in comets and asteroids. Input size distributions of the impactor ensemble correspond to presently observed main belt asteroids and KBOs. Velocity distributions are taken from dynamical simulations for the Nice model. Depending on the composition of large cometary impactors, the Earth could acquire a more massive atmosphere, a few bars in terms of surface pressure, mostly as CO and CO₂. For Mars accumulation of 1–4 bars of CO and CO₂ requires an asteroidal 'late veneer' of the order of 10²⁴ g containing 2% atmophiles.

© 2012 Elsevier Inc. All rights reserved.

1. Introduction

The origin of the primary atmospheres of the terrestrial planets is a consequence of the evaporation of volatiles during catastrophic impacts (Abe and Matsui, 1985; Zahnle et al., 1988, 2007). Initially bodies strike at moderate velocities close to the planetary escape speed but later, when the velocities of small bodies are stirred up, impact erosion is thought to be one of the major loss mechanisms (Zahnle et al., 1992; Ahrens, 1993). Other sources and sinks like volcanic degassing, hydrodynamic and Jeans escape or pick-up of ionospheric particles by the solar wind operate on longer time scales and are only important after the impact rate decreased by orders of magnitude (Zahnle et al., 2007; Kulikov et al., 2007; Boeswetter et al., 2010). A cataclysmic late heavy bombardment about 600 myr after the formation of the planets (Wetherill, 1975; Ryder, 2002) may change the picture. The amount of atmospheric erosion and the retention of volatiles from the impactors during this epoch is crucial and may decide about the habitability of the planet. There

are several hypotheses for the so-called lunar cataclysm or late heavy bombardment (LHB) and for the population of impactors. Already Wetherill (1975) suggested bodies stored beyond the orbit of Neptune, see also Levison et al. (2001). A new idea is the Nice model involving resonant migration of the giant planets (Gomes et al., 2005; Morbidelli et al., 2010). Bottke et al. (2007) investigated the complementary standpoint of a continuously decaying bombardment with the help of dynamical modeling and find that this either over-produces large lunar impact basins comparable to the South-Pole Aitken, or it does not yield the known basins at their time of formation. A quite different scenario has been proposed by Čuk and Gladman (2009), where primordial lunar Trojans are destabilized during early tidal evolution of the lunar orbit, in this case the bombardment is restricted to the lunar surface and to an early time and is unlikely to produce an effect about 600 years after formation the Earth–Moon system. In the Nice model a large fraction of the bodies that strike the terrestrial planets arrives from outer parts of the Solar System, beyond the orbit of Neptune (Gomes et al., 2005), carrying volatiles that have not been present in the asteroid belt and in the feeding zones of terrestrial planets during the accretion era. In particular for the atmospheres of Earth and

* Corresponding author.

E-mail address: detlef.deniem@dlr.de (D. de Niem).

Table 1
Physical mechanisms contributing to atmospheric erosion by impact. Only some of the authors quoted.

Case	Physical effect	Authors
1	Compression and jetting of gas displaced during impactor entry	Walker (1986) Svetsov (2000, 2007)
2	Shock wave caused by plume of partially vaporized impactor and target material	Melosh and Vickery (1989) Zahnle (1990), Newman et al. (1999) Svetsov (2007), Shuvalov (2009) Pham et al. (2009)
3	Global action of the free surface during large impacts	Chen and Ahrens (1997) Genda and Abe (2003)
4	Interaction of high-speed ejecta fragments with atmosphere	Artemieva and Ivanov (2004) Goldin and Melosh (2009) Manning et al. (2009)

Mars this could have had drastic consequences, comparing the total mass of impactors striking the Earth of the order of 2×10^{23} g (Gomes et al., 2005), to the mass of the modern terrestrial atmosphere of about 5×10^{21} g. Mars may have received a comparable amount of material as the Earth, if all large impact basins identified by Frey (2008) formed contemporaneously with the lunar bombardment.

In our model we study the consequences of any heavy bombardment for atmospheres of terrestrial bodies. The significant input parameter is the total cumulative impactor mass. It is unimportant whether this total impactor mass strikes the planetary body in a relatively short interval of 300 myr which is assumed for the LHB or in a longer period, after the formation of a solid crust. Thus we do not require a terminal lunar cataclysm. Our only constraint is that the bombardment is shorter than the time scale of long-term atmospheric loss processes.

For a large meteor impact, such that the object is not considerably decelerated before striking the surface, it has been found that only a small fraction of the impact energy is delivered to the atmosphere by any of the mechanisms listed in Table 1, showing that direct numerical simulation is very difficult. A related problem is that of loss of impactor volatiles from the atmosphere but this has received less attention. Walker (1986) considered the combined effect of shock-compressed air and ablated meteorite material during the entry phase however without describing the final jetting and escape. The so-called vapor plume as it occurs in a terrestrial impact¹ was regarded by Vickery and Melosh (1990) and Zahnle (1990) with the help of a spherically symmetric analytical solution for expansion of a perfect gas into vacuum due to Zeldovich and Raizer (1967). This approach has also been used to estimate the impactor loss. According to more realistic numerical simulations by Svetsov (2007) or Shuvalov (2009) this leads to an overestimate at the Chicxulub scale when comparing results for a 90° impact where Shuvalov (2009) obtained that only an atmospheric mass corresponding to 0.02% of that of a 10 km diameter impactor was lost, for a kinetic energy of 2.75×10^{30} erg. At comparable kinetic energy, for a 7.1×10^{14} g silicatic impactor at 25 km s^{-1} the lost fraction of air given in Table 1 by Vickery and Melosh (1990) corresponds to 3.4% of the impactor, and about 25% of the impactor itself was lost.

On the other hand the average over impact angle by Shuvalov (2009) is comparable: 3% of the impactor mass as escaping air and 20% of the impactor itself. The main contributions in the simulations by Shuvalov (2009) arose from highly oblique, $\leq 30^\circ$ to the horizontal incidence where the Vickery and Melosh (1990) model is not applicable. Korycansky (1992) investigated the propagation of a shock wave in the Kompaneets approximation (Newman et al., 1999) and found a widening of the front into the polar direction with radial distance in 2D spherical coordinates, in a density gradient for power law stratification r^{-n} less steep than $n = 4$, but concentration inside a cone with increasing n . This collimation was also found for an explosion in an isothermal atmosphere by Newman et al. (1999) applying it to an impact of the Chicxulub scale. Svetsov (2000), investigating the small-size threshold where impact erosion becomes inefficient, regarded the meteor entry phase in an analytical pancake model valid during meteorite fragmentation (Hills and Goda, 1993). Genda and Abe (2003), in the opposite limit of very large impacts approximated the motion of the free surface as a solid piston traveling radially in ballistic free-fall and studied the reaction of the atmosphere numerically in a 1D spherically symmetric approximation, neglecting the vapor plume. Later Svetsov (2007) modified his original model to parametrize results of 2D numerical simulations in 1-bar and more massive atmospheres of the Earth and early Mars, additionally he proposed analytical formulas describing loss of impactor and target material. Earlier Svetsov (2003, 2005) also simulated the consequences of 'sterilizing' impacts for the Earth but without including an initial atmosphere, regarding only the impact-produced rock vapor atmosphere. The most extensive 3D hydrocode study investigating atmospheric erosion and impactor retention using realistic equations of state (EOS) is that by Shuvalov (2009); both last authors employ the same hydrocode algorithm SOVA (Shuvalov, 1999). The partition of the impactor kinetic energy converted into either the vapor plume (Vickery and Melosh, 1990), into gas flow expanding outward through the meteor wake (Svetsov, 2000), or into the amplitude of the free surface motion as required by Genda and Abe (2003) is undetermined in simple models that do not take the crater formation into account. The fourth entry in Table 1 would be worth of consideration when the impactor mass is comparable or exceeds that of the entire atmosphere, as it may have occurred several times during the heavy bombardment era.

Pham et al. (2009) regarded impact erosion and delivery of atmospheres solving a deterministic differential equation resembling the model by Zahnle et al. (1992) or Svetsov (2007) backwards in time over an interval of 4.6 Gyr, without special distinction of a heavy bombardment era. The authors apply a scaled version of the Melosh and Vickery (1989) model for atmospheric erosion. Both the ratio of cometary to asteroidal impactors and their velocity distribution correspond to currently existing populations.

The purpose of this work is a Monte Carlo study regarding the effects of atmospheric delivery and erosion during the heavy bombardment era. The input size distributions of the impactor ensemble correspond to presently observed main belt asteroids and KBOs. The input velocity distributions are taken from the Nice model. Considering such different planets as Earth and Mars requires to scale the effects of atmospheric gains and losses due to impacts over a huge interval of impactor diameters, for variable surface pressures, different planetary gravity and radius. Therefore Section 2 critically reviews scaling formulas for atmospheric effects favored by authors such as Shuvalov (2009) and Svetsov (2007) who directly studied atmospheric erosion with the help of hydrocode simulations. A rather simple expression describing atmospheric erosion due the impulse transferred by the free surface of the target planet, regarded with the help of one-dimensional numerical simulations by Genda and Abe (2003) is derived, see

¹ For Mars the present mean impact velocity does not cause complete evaporation.

Eq. (10). For the larger than kilometer-sized bodies that dominate the heavy bombardment era, values do not deviate much from the models by Svetsov (2000, 2007). The impactor loss is described with the help of a model originally due to Zeldovich and Raizer (1967) resembling the approach by Vickery and Melosh (1990). Section 3 provides details of the Monte Carlo model. Results for atmospheric evolution dominated by impacts during the terrestrial and martian heavy bombardment are given in Section 4.

2. Atmospheric erosion and impactor retention

2.1. Recent hydrocode simulations by Shuvalov

Although there is a great number of works devoted to planetary impacts, very few of these are applicable to the problem of atmospheric erosion. Realistic numerical simulations with the help of multi-material hydrocodes using adequate equations of state are those in 3D by Shuvalov (2009), or in 2D cylindrical geometry by Svetsov (2007) using SOVA (Shuvalov, 1999). In Fig. 1 a dimensionless atmospheric erosion efficiency proposed by Shuvalov (2009) is reproduced. The coefficients for the polynomial of 5th order in log–log form are taken from a more recent LPSC abstract (Shuvalov, 2010), see his Eq. (4). Shuvalov (2009) defines erosion efficiency as $(m_a/M)/((v/v_{esc})^2 - 1)$ and assumes that it is a function of a dimensionless energy-like parameter²

$$\chi := \left(\frac{D}{H}\right)^3 \frac{\rho_p \rho_t}{\rho_0(\rho_p + \rho_t)} \max \left\{ \frac{v^2}{v_{esc}^2} - 1; 0 \right\}. \quad (1)$$

Here m_a is the lost atmospheric mass and M that of the bolide, D denotes the impactor diameter, H the atmospheric scale height, ρ_p , ρ_t , and ρ_0 are the densities of meteorite, target and that of the atmosphere at the surface. The impact velocity v has to be larger than v_{esc} , the gravitational escape velocity of the planet.

Fig. 1 is thought as an average over the impact angle distribution (Shuvalov, 2009), and applicable for asteroidal and cometary impactors assuming modern terrestrial conditions for the atmospheres of Earth and more dense atmospheres. For better interpretation of this figure, values corresponding to basaltic impactors of given sizes and velocity of 20 km s^{-1} are also shown. It has to be remarked that Shuvalov (2009) only used diameters from 1 to 30 km for the impactor. His simulation results nearly extend to the right end in Fig. 1 only because of maximum impact velocities of 70 km s^{-1} for comets. The equivalence to impacts of larger objects with moderate velocity only arises if accepting the above scaling law. The behavior for large impactors therefore remains uncertain.

This is indicated by an apparent local maximum of total eroded atmospheric mass for impactors of about 80 km diameter, see Fig. 2, where the dimensionless relation has been converted into dimensionful units assuming an impact velocity of 21 km s^{-1} , close to the mean value for observed NEAs (Stuart and Binzel, 2004), and basaltic composition for both impactor and target. The local maximum is caused by the log–log fit and the assumption of dependence on the energy-like parameter χ . Beyond the local extremum the eroded mass is decreasing in absolute magnitude, see Fig. 2. A local extremum of escaping mass is strange: from other models, see below, one would rather expect it to grow monotonously with impactor size and kinetic energy. An extremum in efficiency occurs at much lower size, see Fig. 1. Certainly it is not allowed to extrapolate Shuvalov's fit as far as done in Fig. 2 but the exercise demonstrates uncertainties for large bodies during the formation of the lunar and martian impact basins.

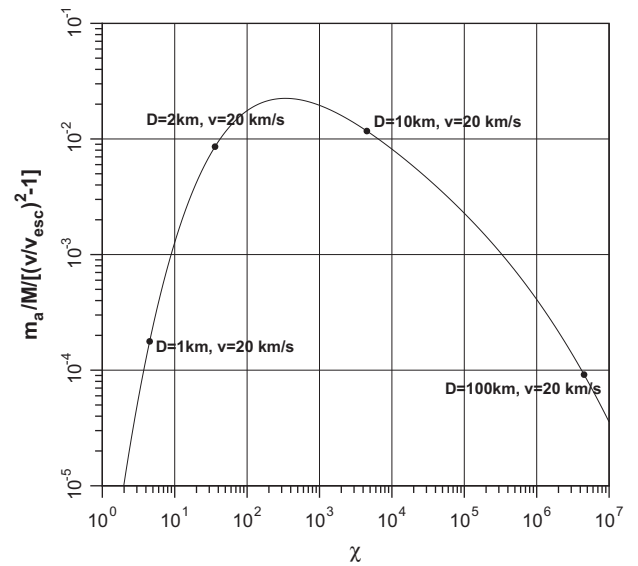


Fig. 1. Dimensionless atmospheric erosion efficiency for terrestrial atmosphere according to Shuvalov (2009). Solid curve: $m_a/M/((v/v_{esc})^2 - 1)$ as function of dimensionless variable χ , see Eq. (1). Symbols: illustrative examples, using Shuvalov's scaling formula, for basaltic impactors (target of same material) at 20 km s^{-1} , and one bar surface pressure.

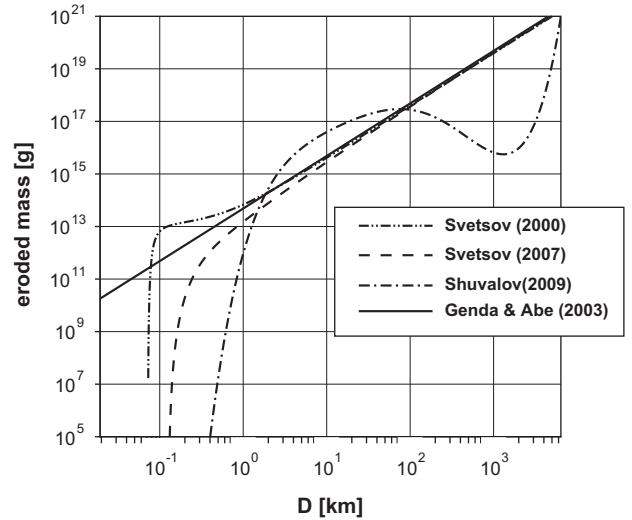


Fig. 2. Eroded atmospheric mass in physical units for a 21 km s^{-1} basaltic impactor, target of the same material and a $T_s = 288 \text{ K}$, 1 bar terrestrial atmosphere. Dash-dotted line: Shuvalov (2009), corresponding to Fig. 1 but severely extrapolated. Dash-dot-dot line: Svetsov (2000), see Eqs. (2) and (3), with correction factor for oblique impact. Dashed line: Svetsov (2007), Full line: model by Genda and Abe (2003), assuming free surface velocity decaying as $\propto r^{-2}$ with $Z = 1.87$ from Tonks and Melosh (1992), using Eq. (10).

2.2. Svetsov's analytical meteor entry model

Svetsov (2000) proposed an analytical model for atmospheric erosion with emphasis on the fragmentation of objects decelerated by the atmosphere but still arriving at the ground with sufficient velocity to cause escape of part of a vapor plume. He obtained an erosion efficiency of

$$\frac{m_a}{M} = \frac{3\rho_0}{4\rho_p} \left(\frac{2H}{D} + \frac{16H^2\rho_0^{1/2}}{3D^2\rho_p^{1/2}} + \frac{16H^3\rho_0}{D^3\rho_p} \right) \left(\int_0^1 (1-x^2)^k dx \right), \quad (2)$$

² Roughly the ratio of the impactor kinetic energy to that of atmosphere in a H^3 cube moving with v_{esc} .

where $x := \min\{1, v_{\text{esc}}/v_\infty\}$ is the ratio of the planetary escape velocity to the asymptotic expansion speed of the vapor plume $v_\infty = v_i \sqrt{4\gamma/(\gamma-1)}$, in terms of the impact speed v_i reached at the ground, and the adiabatic coefficient of the gas γ . The meteor entry velocity v is reduced by drag (Svetsov, 2000)

$$v_i = v \exp\left(-\frac{C_D m_t}{2M}\right), \quad (3)$$

where m_t/M denotes the polynomial in H/D forefactor appearing in Eq. (2) and C_D is the drag coefficient. Svetsov (2000) evaluated the airmass m_t encountered along the trajectory, modified due to projectile spreading in the pancake model by Hills and Goda (1993). The ratio of this mass m_t to that of the meteorite, M , leads to the polynomial in H/D fore-factor in Eq. (2). The escape of gas is modeled with the help of a one-dimensional analytical solution for the free expansion of gas into vacuum where k is related to γ by $k = (3-\gamma)/2(\gamma-1)$ (Svetsov, 2000). We use a value of $k = 5$ corresponding $\gamma = 13/11$, suggested by (Svetsov, 2007). Only a fraction of the traversed airmass m_t escapes, given by the x -dependent quotient of integrals in Eq. (2).

Later Svetsov (2007) modified his original model and used it as a fit for simulation results. Fig. 2 is a comparison of these models, assuming a basaltic $\rho_p = 2.7 \text{ g/cm}^3$ asteroid striking the Earth at 21 km s^{-1} . The mass of the one-dimensional vapor plume is identified with that of the air encountered during the pancake phase, without actually regarding the energy transfer. In a low-pressure atmosphere the result is a very efficient escape, close to the limit set by energy conservation, see Fig. 3. Contrary to physical expectations, the new model (Svetsov, 2007) does not lead to a decrease of the cutoff diameter in a low-density atmosphere, comparing Fig. 3 to Fig. 2.

For impactors considerably larger than $(\rho_0/\rho_p)^{1/3}H$, in Eq. (2) only the term with H/D is important such that in this limit $m_a/M \propto \rho_0 H/(\rho_p D)$, analogous to the model by Genda and Abe (2003), see Eq. (10) below. Differences of 2D vertical to 3D oblique impact simulations are absorbed into a constant enhancement factor, here Svetsov (2007) proposed to integrate the function $(1+2\sin(2\alpha))^2$ over impact angle distribution $\sin(2\alpha)d\alpha$ in the interval $\{0, \pi/2\}$. In Fig. 2 this correction factor $f_x = \int_0^{\pi/2} d\alpha (1+2\sin(2\alpha))^2 \sin(2\alpha) = 5 + \pi - 4/3$ has been applied.

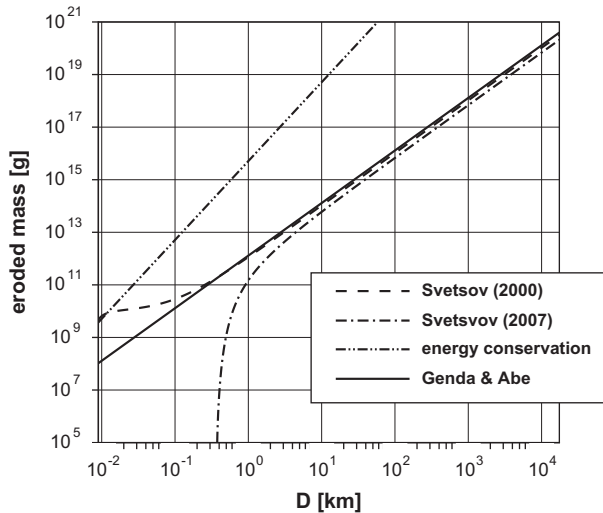


Fig. 3. Atmospheric mass eroded during Mars impact of stony asteroids vs. diameter D . Martian atmosphere with 0.01 bar. Impact velocity 9.6 km s^{-1} , average for present asteroidal population (Ivanov, 2001). Dash-dotted line: Svetsov (2007), Dashed line: Svetsov (2000), Full line: Genda and Abe (2003) model, Dash-dot-dot line: energy conservation limit assuming 100% impactor energy conversion into escaping gas with $v = v_{\text{esc}}$.

2.3. Genda and Abe: loss induced by free surface motion

In large impacts during the heavy bombardment era the effect of the free surface regarded by Genda and Abe (2003) cannot be neglected. The region where the atmospheric gas is lost has been found with the help of tracer particles in the simulations by Svetsov (2007), see also Shuvalov (2009) or Hamano and Abe (2006). A qualitatively similar conical loss region emerges from the Genda and Abe (2003) model: with decreasing velocity at the free surface, the initial altitude of the escaping part of the atmosphere increases until the amount of mass becomes negligible at some distance from 'ground zero'. One-dimensional spherical numerical calculations by Genda and Abe (2003) led to the approximation of the local erosion efficiency, defined as local mass fraction of ejected atmospheric mass, as

$$\chi_{\text{loss}} = \min\left\{1, \frac{4v_s - v_{\text{esc}}}{3v_{\text{esc}}}\right\}, \quad (4)$$

where v_s is the local free surface velocity, there is zero loss when $v_s \leq v_{\text{esc}}/4$. If z denotes the lower limit of the initial altitude of the lost gas fraction it corresponds to a point on the geometric boundary of the loss region. Assuming an isothermal atmosphere this altitude is given by

$$\exp\left(-\frac{z}{H}\right) = \frac{4v_s(s) - v_{\text{esc}}}{3v_{\text{esc}}}, \quad (5)$$

here s is the distance from ground zero to the corresponding surface point. This follows from the assumption by Genda and Abe (2003) that the effect is caused by a local, radially outward motion of the surface. The free-surface velocity is assumed to decrease as a power law: $v_s = v_{\text{esc}}(s/s_{\text{esc}})^{-Z}$, where s_{esc} is the distance where the surface ejection velocity exceeds the escape threshold. $Z = 2.5$ is typical for craters in rock and sand, $Z = 1.7$ has been found for liquid water (Schmidt and Housen, 1987; Holsapple and Schmidt, 1987). During early stages of an impact the pressure distribution can be approximated such that a spatially constant central region exists, called the isobaric core, whereas the pressure rapidly decreases outside this region (Tonks and Melosh, 1992). The last authors prefer $Z = 1.87$ close to the isobaric core. Care is necessary: the exponent Z related to crater scaling laws by Schmidt and Housen (1987) corresponds to the point-source limit of crater formation and to late-time effects in laboratory experiments. It is not valid for early-time cavity growth close the isobaric core, see also Housen and Holsapple (2010). For given altitude z of a point on the outer boundary of the region of escaping atmospheric gas, Eq. (5) determines the distance from ground zero to the corresponding ground point

$$s(z) = s_{\text{esc}} \left[\frac{1}{4} + \frac{3}{4} \exp\left(-\frac{z}{H}\right) \right]^{-1/Z}. \quad (6)$$

To evaluate the atmospheric mass in the loss region, first we approximate the planetary surface locally as flat such that s is a cylindrical coordinate, measured along the surface. Elementary integration determines the mass

$$m_a = \pi \rho_0 \int_0^\infty s^2(z) \exp(-z/H) dz = \frac{Z[4 - 4^{2/Z}]}{3(Z-2)} \pi s_{\text{esc}}^2 H \rho_0. \quad (7)$$

For comparison we also regard the true situation in spherical coordinates. Assuming that ground zero is on the planetary surface the chord length s is related to the polar angle by $s = 2R \sin \vartheta/2$. The angle ϑ is the co-latitude of the surface point from that the local altitude of the loss cone is measured. With the help the cosine addition theorem one finds

$$1 - \cos \vartheta = 2 \left(\frac{s(z)}{2R} \right)^2, \quad (8)$$

where $s(z)$ is given by Eq. (6). Using the fact that $r = R + z$ is the spherical radial coordinate the airmass in the region occupied by the loss cone is

$$m_a = 2\pi\rho_0 \int_0^\infty (R+z)^2 (1 - \cos\vartheta(z)) \exp(-z/H) dz$$

$$= \pi\rho_0 s_{esc}^2 H \int_0^\infty \frac{(1 + \frac{H}{R}u)^2 \exp(-u) du}{(1/4 + 3/4 \exp(-u))^{2/Z}}, \quad (9)$$

where the substitution $u = z/H$ has been made. Neglecting terms of order H/R in the numerator the previous result, Eq. (7) is recovered. Actually Genda and Abe (2003) simulated one-dimensional motion for initially adiabatic stratification. Assuming an adiabatic atmosphere does not change the final result in terms of scale height, see Appendix A.1. The velocity at the free surface above the target portion of the isobaric core equals the impact velocity because of approximate doubling of the particle speed if projectile and target are of the same material (Melosh, 1989). This allows to find the distance where the free-surface velocity drops below the escape threshold such that the locally flat approximation Eq. (7) leads to

$$m_a = \frac{2^{2/3} Z [4 - 4^{2/Z}]}{12(Z-2)} \pi D^2 H \rho_0 \left(\frac{v}{v_{esc}} \right)^{2/Z}. \quad (10)$$

In the derivation we have set $s_{ic} \approx 2^{1/3} D/2$ as the distance of the isobaric core following Tonks and Melosh (1992), see also Senshu et al. (2002). We prefer the value of $Z = 1.87$ by Tonks and Melosh (1992) although the dependence of the fore-factor on Z is not very strong. The Z -dependent factor multiplying $\pi s_{esc}^2 H \rho_0$ in Eq. (7) is (2.094, 1.614, 1.480) for $Z = 1.7$, $Z = 2.5$, $Z = 3$, respectively. The situation is more complicated if v_{esc} is not even reached by the ejection speed inside the isobaric core. With the help of Eq. (5) then the region of lost air begins at a nonzero altitude of $z = H \ln[(3v_{esc}/(4v - v_{esc}))]$, still assuming that the maximum ejection speed exceeds $v_{esc}/4$. This can be shown after considerable algebra to lead to

$$m_a = \frac{2^{2/3} Z [4(v/v_{esc})^{1-2/Z} - 4^{2/Z}]}{12(Z-2)} \pi D^2 H \rho_0 \left(\frac{v}{v_{esc}} \right)^{2/Z}. \quad (11)$$

As required the fore-factor vanishes for $v = v_{esc}/4$ and the velocity dependence is changed but not the scaling with impactor diameter. The lost fraction of the atmosphere is insensitive to the initial conditions (Genda and Abe, 2003) because the product $H\rho_0$ is canceled when dividing by the total atmospheric mass $4\pi R^2 H \rho_0$. The loss cone remains geometrically similar: the enclosed atmospheric mass is proportional to $D^2 H$. For a large 100 km diameter basaltic impactor at 20 km s^{-1} , the lost mass is about a factor of about 1.42 larger than in Shuvalov's description, see Fig. 2, about 1.18 and 1.32 larger than the value due to Svetsov (2000, 2007), respectively. At the $D = 10 \text{ km}$ scale the value from Eq. (10) reaches only about 12% of that by Shuvalov (2009), but it exceeds that due to Svetsov (2000) and Svetsov (2007) by factors of about 1.13 and 1.74, respectively. The ratio of lost atmospheric to impactor mass is decreasing with impactor size $\propto H/D$ as is also true for the Svetsov (2007) model, in the large D limit, see Fig. 2. For the impact of a 6000 km diameter basaltic body at 18 km s^{-1} thought as applicable for the impact origin of the Moon 28.4% of the pre-impact atmosphere would be lost, using Eq. (10), and this is insensitive to the surface pressure and even valid for a curved target surface, neglecting small terms of $O(H/R)$. Nevertheless this conclusion seems to be questionable and fully realistic simulations with a pre-existing atmosphere would be required, also because the model does not take into account the geometry of more complicated oblique impacts.

Assuming that the lost gas moves with v_{esc} at least, using Eq. (10) energy conservation is violated when

$$D \leq \frac{2^{2/3} Z [4 - 4^{2/Z}]}{2(Z-2)} \frac{P_s}{g_s \rho_p} \left(\frac{v}{v_{esc}} \right)^{2/Z-2}, \quad (12)$$

using $\rho_0 H = P_s/g_s$ for an isothermal atmosphere (Manning et al., 2009). For the present atmosphere and a stony meteorite this D corresponds to 9.1 m at 20 km s^{-1} , such objects would be severely decelerated or destroyed during atmospheric entry, already. Although this difficulty does not appear in the models by Svetsov (2000) and Svetsov (2007), there is a comparable problem to determine a decrease of the effect with impactor diameter in low-density atmospheres, see last subsection.

2.4. Loss of impact-created vapor and retention of the impactor

Vickery and Melosh (1990), see also Zahnle (1990) introduced a model for the loss of both vaporized impactor and target material and atmospheric gas. Concerning atmospheric erosion the Vickery and Melosh (1990) model is characterized by the fact that there is a limiting impactor size where all atmospheric mass contained above a plane tangent to the surface at the impact site is lost, Vickery and Melosh (1990) found a threshold impactor mass of about $5m_{tan}$, here $m_{tan} \approx 2\pi\rho_0 R H^2$ (Manning et al., 2009). Hydrocode calculations have revised the impactor mass for erosion of this amount by orders of magnitude upwards (Svetsov, 2007; Shuvalov, 2009). For larger sizes the efficiency decreases as $m_{imp}^{-1} \propto D^{-3}$, much steeper than in models by Walker (1986), Genda and Abe (2003), and Svetsov (2007). Note that this argument depends on the validity of the spherically symmetric solution by Zeldovich and Raizer (1967) whereas in reality the vapor plume expands further along the curved surface. These effects hardly can be separated from the acceleration of gas by the free-surface motion regarded by Genda and Abe (2003).

The model by Vickery and Melosh (1990) additionally provides an estimate of the lost fraction of the impactor in the absence of an atmosphere. In a planar impact approximation (Melosh, 1989) the particle velocity is $u_p = v/2$ disregarding impedance matching for unequal target and impactor materials. The total energy per unit mass of the vapor going into free expansion is $E/M = \epsilon - e_{vap}$ where the internal energy is $\epsilon = u_p^2/2$ and e_{vap} is the energy of complete evaporation, for example $e_{vap} = (18(1 - x_{H_2O}) + 3.04x_{H_2O}) \text{ kJ/g}$ for a body with a fraction x_{H_2O} by mass of water, allowing to interpolate in between asteroids and comets, using Tillotson parameters ϵ_{cv} for the energy of complete evaporation (Melosh, 1989) in the case of water and granite. Other rock materials have $e_{cv} = 16 - 18 \text{ kJ/g}$ similar to granite. This estimate for the energy per unit mass neglects the kinetic energy of shocked material $u_p^2/2$ and implicitly assumes an energy partition of 1:1 between vapor plume and crater formation.

The asymptotic velocity at the outer boundary in the analytical solution by Zeldovich and Raizer (1967) for free expansion of a gas into vacuum is

$$v_\infty^2 = (2k + 5) \frac{2E}{3M}, \quad (13)$$

where k is the exponent in $\rho \propto R^{-3}(1 - x^2)^k$ for the density, $x = r/R$, and $R = R(t)$ is the radius at the outer edge, E and M are the total energy and mass, respectively (Zeldovich and Raizer, 1967), see also Vickery and Melosh (1990). The radial velocity is a linear function of r so the mass fraction with $v_r > v_{esc}$ can easily be found (Vickery and Melosh, 1990; Zahnle, 1990)

$$\zeta := \frac{m(x)}{M} = C \int_x^1 x^2 (1 - x^2)^k dx, \quad (14)$$

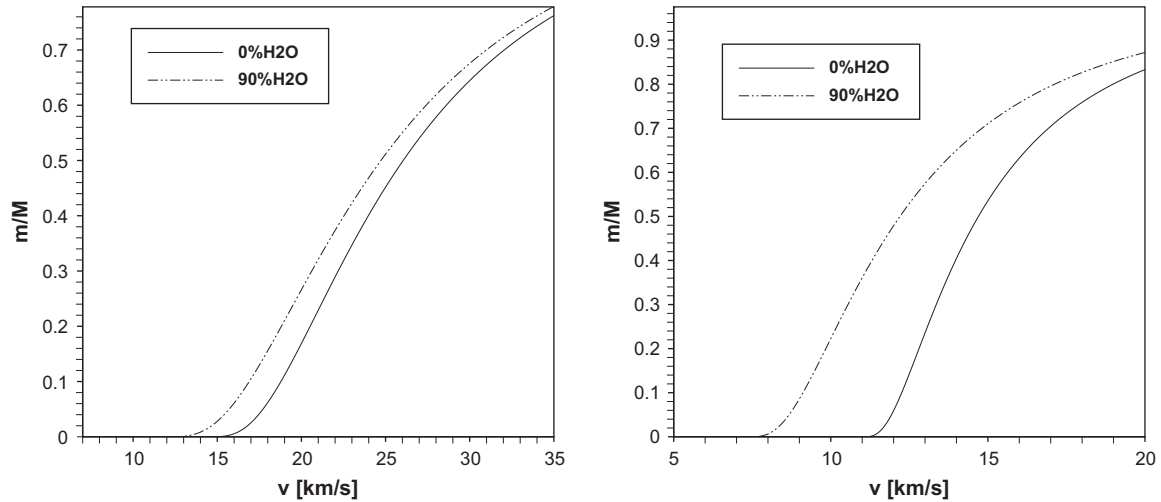


Fig. 4. Escaping impactor mass fraction, Eq. (14) for $\gamma = 1.2$ and variable water content by mass, $x_{\text{H}_2\text{O}}$. Left: terrestrial case without atmosphere. Right: case of Mars. Average impact velocities of present Mars crossers: 9.6 km s^{-1} (Ivanov, 2001).

where $x = v_{\text{esc}}/v_{\infty} \leq 1$ and $C = 2/B(3/2, k + 1)$ in terms of the Beta function normalizes the expression to unity. The integral can be given analytically in some cases, see Appendix A.2. The parameter k is fixed for spatially constant specific entropy as $k = 1/(\gamma - 1)$ (Zeldovich and Raizer, 1967). The value of k is arbitrary if the entropy is allowed to be spatially variable. There is no other preferred value of k , we only use $k = 1/(\gamma - 1)$ here. An analytical solution where the internal energy is spatially constant, initially, does not exist, so there is no reason to prefer a different value of k . Fig. 4 (left part) shows the impactor loss for the terrestrial case assuming $\gamma = 1.2$ that comes closer to reality than $\gamma = 1.4$, for hot and dense vapors with many internal degrees of freedom. Fig. 4 (right part) shows the same calculation for Mars. The average impact velocity of present Mars-crossing asteroids is only 9.6 km s^{-1} (Ivanov, 2001), so Fig. 4 would suggest that volatiles delivered by these and bodies on similar orbits are retained. To describe how a dense atmosphere prevents the free expansion into vacuum, an approximation is to introduce a limiting impactor mass above that Eq. (14) is regarded valid, and below that ζ is set to zero. Along the lines of this model one has to assume a multiple of the tangent-plane mass m_{tan} for the limiting impactor.

In the case of large enough impactors where Eq. (14) is applicable it moderately overestimates losses compared to realistic hydro-code simulations by Shuvalov (2009), averaged over the impact

Table 2

Lost fraction of atmosphere m_a/M and impactor m_p/M in terrestrial impacts of asteroids and comets from Shuvalov (2009), valid as average over impact angle distribution. Last two columns: theoretical impactor loss fraction ζ_v , Eq. (14) due to Vickery and Melosh (1990) ($\gamma = 1.2$, $\epsilon_{\text{vap}} = 12.37 \text{ kJ/g}$ for asteroids) and ζ_s due to Svetsov (2007).

Body	D (km)	v (km/s)	m_a/M	m_p/M	ζ_v	ζ_s
Asteroid	1	15	$1.e-5$	0.0	0.0	0.0
Asteroid	3	15	0.01	$4.e-4$	0.0	0.0
Asteroid	10	15	0.01	0.06	0.0002	0.0
Asteroid	30	15	$4.e-3$	0.07	0.0002	0.0
Asteroid	1	20	$3.e-4$	0.0	0.0	0.0
Asteroid	3	20	0.029	0.03	0.0	0.0
Asteroid	10	20	0.03	0.2	0.168	0.0
Asteroid	30	20	$5.e-3$	0.1	0.168	0.0
Comet	1	30	0.011	0.0054	0.0	0.0
Comet	3	30	0.21	0.38	0.0	0.00003
Comet	10	30	0.07	0.47	0.679	0.00013
Comet	30	30	.017	0.53	0.679	0.005

angle distribution, see Table 2, sixth column except for rather low velocities of 15 km s^{-1} that are not typical for a Nice model type of the LHB. In one case – for a 10 km diameter asteroid and 20 km s^{-1} – numerical results of Shuvalov (2009) yield a slightly larger impactor loss however the case of the larger 30 km diameter asteroid at the same velocity gives a factor of two smaller loss, therefore comparison with these two numbers is problematic. The last column additionally gives the lost impactor fraction according to Svetsov (2007), (calculated using his Eq. (5)). Most of cometary volatiles during a terrestrial heavy bombardment era will be retained following the numerical results by Shuvalov (2009). The analytical model, Eq. (14) with $\gamma = 1.2$ approximates the numerical values in the region between 20 and 30 km s^{-1} whereas for 15 km s^{-1} it underestimates them. The characteristic impactor size above that the atmosphere is unimportant is so large that the effect at 3 km diameter is set zero here. Below the threshold diameter we introduce an additional term that evaluates the impactor loss differently, proportional to the lost atmospheric mass, see next section.

3. Monte Carlo approach

Now we outline a Monte Carlo model for the change of the atmosphere by an impact of an asteroid or comet. Atmospheric erosion is described here with the model of Svetsov (2000) corrected for the effect of impact angle as described above, see Chapter 2.2. The reason to prefer this version is that it does not contain the 8 additional parameters ($C_{2, \dots, 5}$ and 4 additional exponents) of its more recent version (Svetsov, 2007) and the small-size cutoff behaves physically more correctly with changing atmospheric pressure, see Fig. 3. Impactor retention is treated with the model described in Chapter 2.4, additionally we use the idea by Svetsov (2007) about a proportionality between lost impactor and atmosphere mass below a threshold size. After n impacts the total mass of the planetary atmosphere shall be $m_{a,n}$. The following $(n + 1)$ th impact leaves a total atmospheric mass

$$m_{a,n+1} = m_{a,n} + \delta m_{a,n}. \quad (15)$$

The mass change $\delta m_{a,n}$ is made up of several contributions discussed in Section 2 already. We itemize these contributions below. Velocity and size frequency (SFD) distributions of the impactors are generated to correspond to the Nice model (Gomes et al., 2005; Morbidelli et al., 2010). The composition is a free parameter with

regard to different variants of the Nice model where composition here is understood as the ratio of comets vs. asteroids. We create different ensembles of Near Earth Objects and martian impactors to investigate the evolution of the terrestrial and martian atmospheres.

In the following we list the contributions to the mass change $\delta m_{a,n}$. First we split

$$\delta m_{a,n} = \delta m_{a,n}^{(+)} - \delta m_{a,n}^{(-)}, \quad (16)$$

where $\delta m_{a,n}^{(+)}$ is a net replenishment term originating from impactor material whereas $\delta m_{a,n}^{(-)}$ describes loss of preexisting atmospheric gas. The replenishment term $\delta m_{a,n}^{(+)}$ is the amount of material of the projectiles $x_v m_{imp}$ remaining as volatiles in the atmosphere, reduced by the fraction ζ , that escapes during the impact

$$\delta m_{a,n}^{(+)} = x_v m_{imp} - \zeta x_v m_{imp} = (1 - \zeta) x_v m_{imp}, \quad (17)$$

where m_{imp} is the mass of the $(n + 1)$ th impactor and the loss fraction ζ has been introduced in Eq. (14) above, subscripts n on the right hand side of Eq. (17) have been dropped. Outgassing of the target is neglected for simplicity although this is an additional source of atmospheric gases in a large impact. Erosion is described with the help of $\delta m_{a,n}^{(-)} = \eta m_{imp}$ where the efficiency η still depends on parameters characterizing the impactor and atmosphere. The erosion efficiency η may be taken either as that due to Svetsov (2000, 2007) or Genda and Abe (2003) given in Section 2. A subscript n for η is again dropped. The stochastic evolution of the atmospheric mass now is given by

$$m_{a,n+1} = m_{a,n} + ((1 - \zeta)x_v - \eta)m_{imp}. \quad (18)$$

The escaping fraction ζ of the impactor mass significantly depends on the size but above some threshold impactor size D_{lim} any previous atmosphere has only a small effect, and ζ becomes independent of atmospheric properties. In this limit ζ is that given by Eq. (14) above. Below the threshold size the impactor loss is proportional to the lost atmospheric gas (Svetsov, 2007)

$$\zeta = \Phi \eta, \quad D < D_{lim}, \quad (19)$$

where Φ is approximated by a constant and the limiting impactor size determined by $\pi \rho_p D_{lim}^3 / 6 = 2\pi \rho_0 R H^2$ corresponding to the tangent plane mass. Svetsov (2007) evaluated the impactor loss as equivalent to the lost airmass at 0.35 of the impactor's diameter. We simply set $\Phi = 1/0.35 \approx 2.857$, see Table 3, because Svetsov's erosion efficiency roughly is inversely proportional to impactor diameter, except for very small objects near the cutoff size. For comparison, the result by Shuvalov (2009) for a 10 km diameter asteroid at 45° corresponds to $\Phi = 2.5$. Svetsov (2007) additionally assumes a velocity dependence $\Phi \propto v^{-1/4}$ but with the consequence that the amount of lost projectile material in proportion to atmospheric mass is decreasing for larger impact velocities. Such a velocity dependence is not included here, partly because in this way we obtain an upper limit for the loss of smaller-than-threshold impactors. Moreover η already contains the effect of atmospheric pressure on the loss. This implicitly assumes that the amounts of vapor lost from the projectile, target or of atmospheric origin all depend on the surface pressure and impact velocity in the same way.

We generate random impactor sizes corresponding to a model size frequency distribution (SFD) given in the form of the number of objects contained in discrete bins where the bounding diameter of subsequent bins increases by a constant factor,³ typically $\sqrt{2}$ for Kuiper belt objects and $10^{1/10}$ for asteroids. The binned model SFDs for the Kuiper and main belts were constructed to resemble the observed distributions.

³ Except for the largest-sized bin.

Table 3
Input parameters.

Parameter	Earth	Mars	Comment
Total impactor mass (g)	2×10^{23}	$1.8, \dots, 2.3 \times 10^{23}$	Due to Monte Carlo approach total mass slightly varies around these numbers
Initial atmospheric pressure (bar)	1	0.01, ..., 1	Free parameter
Mass ratio cometary/asteroidal %	10, ..., 90	5, ..., 95	Free parameter
Relative mass of atmophile molecules in comets	0.1, ..., 0.3	0.1, ..., 0.3	Eq. (14)
Relative mass of atmophile molecules in asteroids	0.02	0.02	Eq. (14)
Scale height H (km)	8.5	11.9	See Eqs. (1) and (16), derived from present atmospheric conditions
Φ	2.857	2.857	See Eq. (16)
Minimum impactor diameter (m)	76	76	

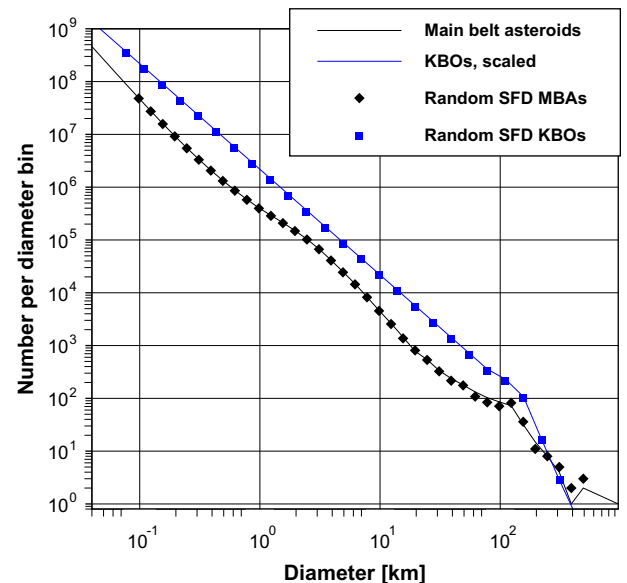


Fig. 5. Random-number-generated SFD compared to the model by Bottke et al. (2005) for present main belt asteroids as input. Diameter ratio of bins $10^{1/10}$ for the input size distribution, except at largest sizes. Also shown is the input model for KBOs in comparison with the random-number-generated SFD for these, however absolute numbers are scaled to fit into the same diagram.

Fig. 5 compares the input SFD with that of a typical random ensemble of impactors generated to resemble the present main belt asteroids where the model by Bottke et al. (2005) for main belt asteroids is used as an input. Also shown is a comparison between a model SFD fit to observations of Kuiper belt objects (Morbidelli et al., 2009) and the random ensemble generated to represent these, however in the latter case the input distribution has been scaled down in absolute number by a large factor to fit into the same diagram. Uniformly distributed random numbers

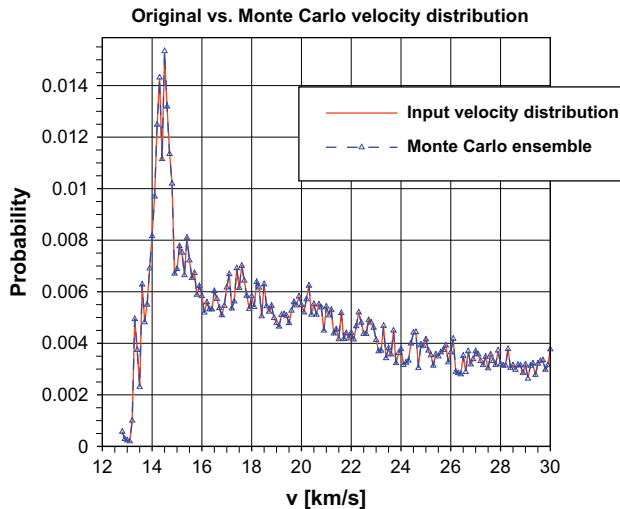


Fig. 6. Blue: random-number-generated distribution of velocities weighted by impact probability during terrestrial heavy bombardment era, for asteroidal component vs. Earth. Gravitational focussing included. Red: input velocity distribution using velocity bins of 0.1 km s^{-1} width. (For interpretation of the references to color in this figure legend, the reader is referred to the web version of this article.)

are mapped into sizes with the help of the inverse of the cumulative SFD. Inversion is straightforward if the cumulative SFD is assumed as a piecewise power law. We used the 64 bit version of the Mersenne Twister (Matsumoto and Nishimura, 1998; Nishimura, 2000) as input pseudo random number generator with uniformly distributed random numbers in $(0; 1]$. In addition to the impactor SFD, their velocity distribution is another model input. The random-number generated impact velocity distributions are compared to the input probability distributions in Figs. 6 and 7. The somewhat spiky appearance of the input velocity distributions is not so much due to dynamics but instead statistical fluctuations that are unavoidable given the width of velocity bins ($=0.1 \text{ km s}^{-1}$) and the finite number of bodies in the dynamical simulations that contribute to the impact probability for a given terrestrial planet.

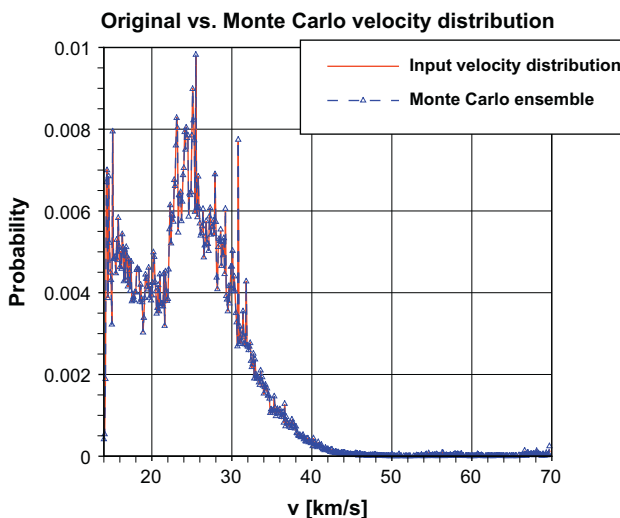


Fig. 7. Blue: random-number-generated distribution of velocities weighted by impact probability during terrestrial heavy bombardment, for cometary component vs. Earth. Red: input velocity distribution. (For interpretation of the references to color in this figure legend, the reader is referred to the web version of this article.)

4. Results for atmospheric evolution during a heavy bombardment phase on Earth and Mars

To simulate the effect of impacts on the atmospheres of terrestrial planets during a heavy bombardment according to the methods described in the previous chapters we distinguish two classes of impactors: asteroids and comets. The impactor classes differ in several properties that are relevant for the atmospheric evolution of the target.

4.1. Composition

We consider here the relative amount x_v of volatiles like CO, CO₂ and other minor atmosphere constituents that can potentially form a stable atmosphere. H₂O does not belong to this class since it rains out following episodic steam atmospheres accompanying very large impacts within 300 to a few 1000 years (Sleep et al., 1989; Zahnle and Sleep, 1997). A cometary number for x_v can be derived from measurements at several comets as Hale-Bopp and Hyakutake where the sum of CO and CO₂ abundances are between 30% and 40% relative to water (Altwegg et al., 1999). The ratio of volatile to refractory matter in comets is quite diverse and assumed to be around one (Sanzovo et al., 2009). We consider here x_v in a range between 10 and 30%. For asteroids most carbon is chemically bound in the form of carbonates and as organic compounds and will be degassed during the impact in high-pressure decomposition reactions. Values of 1–5% for C by mass may be regarded as typical for carbonaceous chondrites (Grady and Wright, 2003). Chemical equilibrium models (Schaefer and Fegley, 2010) predict up to 70% CO₂ in impact-produced atmospheres resulting from CV chondrites however this is an upper limit and the composition depends on meteorite type and temperature. We boldly assigned an average value of 2% for x_v here, typical for C-type asteroids (Grady and Wright, 2003).

4.2. Velocity distributions

The velocity distributions for asteroids and comets crossing the orbits of Mars and Earth are taken from the Nice model and are assumed to be constant over time for each population. Examples were given in Figs. 6 and 7.

4.3. Size distributions

The simulated size distributions of the impactor classes correspond to presently observed main belt asteroids and KBOs. The Monte Carlo model assumes that the size distribution does not change with time. The minimum impactor diameter is about 76 m for KBOs. To this size the bodies barely contribute to atmospheric erosion in the Svetsov (2000) model, and not at all in the modified version (Svetsov, 2007), or that due to Shuvalov (2009), see Fig. 2.

4.4. Mass ratio of impactor classes and initial atmospheric pressure

A question that has not been finally resolved by the Nice model is the mass ratio of comets and asteroids that hit Earth and Mars, respectively. New results to comet Hartley 2 (Hartogh et al., 2011) show that even comets may have a D/H ratio compatible with that of the oceans on Earth. Therefore, the often given preference to asteroidal impactors cannot be justified with this isotopic ratio. Another open issue is the initial atmospheric mass before the bombardment started. Therefore we treat these numbers as free parameters.

4.5. Total impactor mass

Even the total impactor mass that hit Earth and Mars, respectively, during a (late) heavy bombardment era is a matter of controversial discussions (Levison et al., 2001; Ryder, 2002; Dauphas, 2003; Koeberl, 2003; Marty and Meibom, 2007; Bottke et al., 2007; Frey, 2008; Jørgensen et al., 2009). It can be derived by impact basin counting and the use of scaling laws but this provides only rough estimates because of the unknown ages. For Earth we use a value of $M = 2 \times 10^{23}$ g close to that of 1.8×10^{23} g by Gomes et al. (2005) whereas for example the number given by Jørgensen et al. (2009) as 10^9 g falling on each square metre of the Earth's surface would translate into 5×10^{23} g (the surface of the Earth being 5.1×10^{14} m²). The mass according to Levison et al. (2001) is close to 10^{23} g; this rather is a minimum taking into account only Nectarian- and younger age lunar basins and assumes average gravitational focusing. Since appropriate numbers for Mars are missing we made our own analysis (see Appendix A) and found a range of $1.8\text{--}2.38 \times 10^{23}$ g. Values for the total accumulated mass of impactors are highly uncertain and the limit for the total mass accumulated contemporaneously to the terrestrial Late Heavy Bombardment as occurring in the Nice model is considerably lower: about 2×10^{22} g. However 90% of the large martian impact structures according to Frey (2008) would have to be much older than 3.9 Gyr then.

The main differences between the action of impacts on the atmospheres of Mars and Earth result from.

- the different planetary masses that cause the gravitational focusing and the escape velocity,
- the different velocity distributions of the impactor classes at the orbits of both planets,
- the initial pressure of the atmospheres.

Table 3 summarizes the input parameters and their ranges applied in the simulations. Results of the Monte Carlo simulations are given in the following figures.

Fig. 8 shows the pressure evolution for the Earth during the heavy bombardment in dependence on the accumulated impactor mass

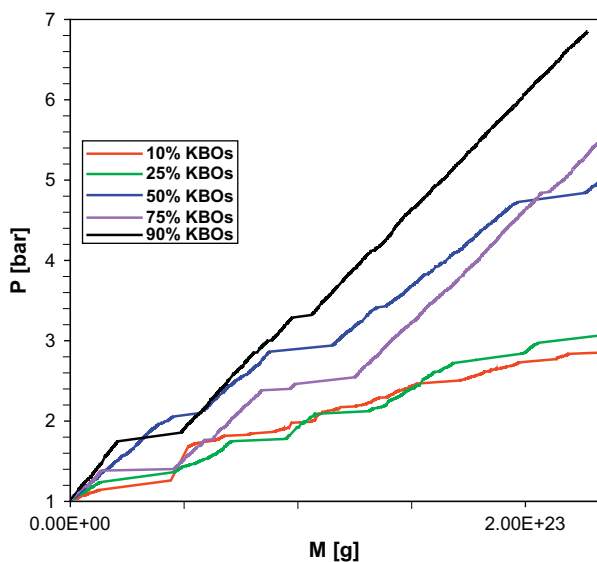


Fig. 8. Terrestrial atmospheric pressure evolution during a heavy bombardment era in dependence on total impactor mass hitting the Earth. Colors represent different mass ratios of KBOs containing $x_v = 30\%$ volatiles to asteroids with $x_v = 1\%$. Each curve averages results of 50 runs. Initial pressure: 1 bar. (For interpretation of the references to color in this figure legend, the reader is referred to the web version of this article.)

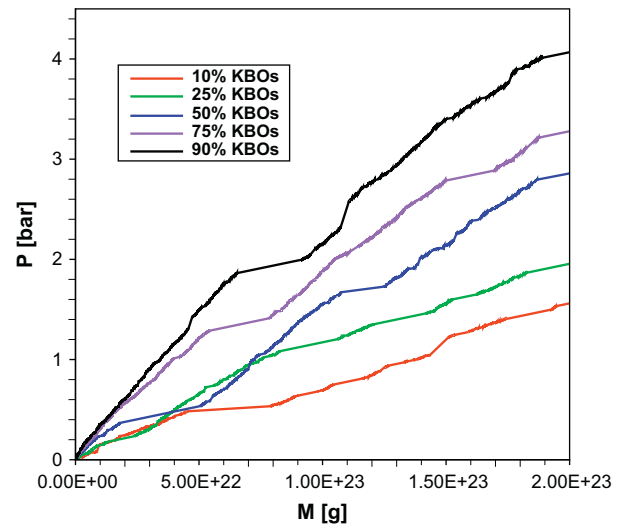


Fig. 9. Same as Fig. 8 but for conditions on Mars. Initial pressure: 0.01 bar. Current dynamical simulations for the Nice model LHB predict a total impactor mass of 2×10^{22} g only. (For interpretation of the references to color in this figure legend, the reader is referred to the web version of this article.)

for varying ratios of KBOs and asteroids. An initial atmospheric pressure of 1 bar is assumed. Each curve represents the average of 50 runs. It is found that the pressure increases with the number of impacts. That means that in the average the retention of new volatiles from the impactors is more prominent than the losses of the existing atmosphere by erosion. This is due to their high content of atmospheric gases. However, sometimes statistical effects break this general rule even after averaging the result of 50 runs. The isolated appearance of rather fast and very massive, volatile-poor asteroids temporarily leads to substantial atmospheric erosion.

Fig. 9 shows the same scenario as given in Fig. 8 but for Mars and with a lower initial pressure of 0.01 bar. The results are similar to those for Earth. The final pressure at the end of the heavy bombardment era is comparable to that on our home planet although

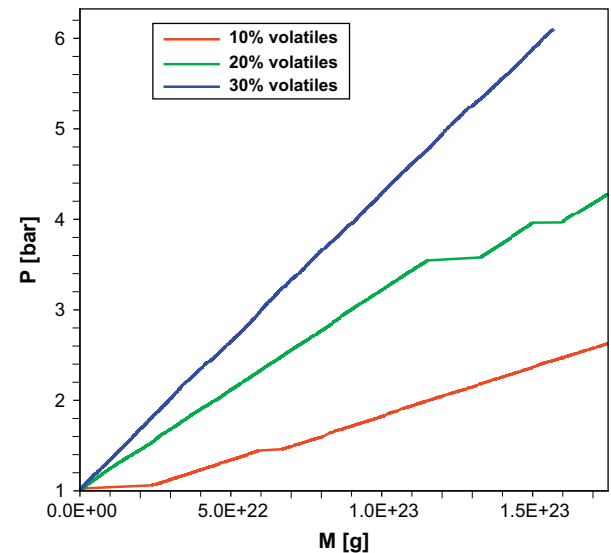


Fig. 10. Terrestrial atmospheric pressure evolution during heavy bombardment in dependence on total impactor mass. Only KBOs are considered. Colors represent different impactor content of atmosphile (CO , CO_2) molecules. Each curve averages results of 50 runs. Initial pressure: 1 bar. (For interpretation of the references to color in this figure legend, the reader is referred to the web version of this article.)

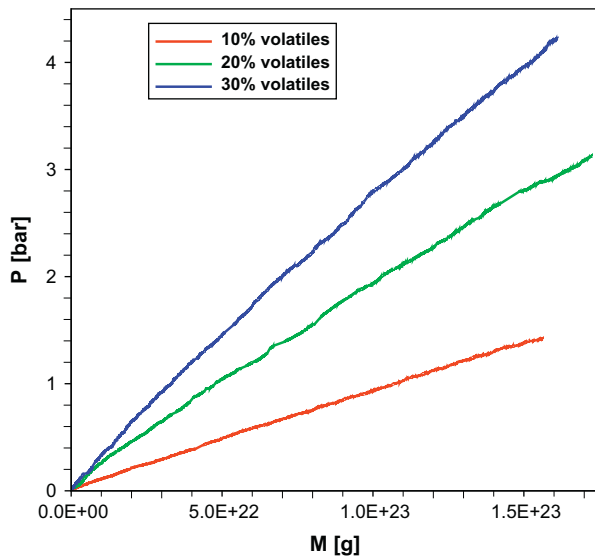


Fig. 11. Same as Fig. 10 but for conditions on Mars. Initial pressure: 0.01 bar. (For interpretation of the references to color in this figure legend, the reader is referred to the web version of this article.)

any volcanic outgassing of CO_2 that mostly took place during first 500 myr on Mars and may add about 500 mbars (Grott et al., 2011) has been completely neglected.

The effect of the composition of KBOs is shown in Figs. 10 and 11, for Earth and Mars, respectively. Fig. 12 displays results for an extremely massive bombardment of Mars with a total impacting mass accounting for all large martian impact basins including a possible martian dichotomy-causing body but for a population dominated by 99% relatively volatile-poor $x_v = 2\%$ asteroids. To give an idea of the magnitude of fluctuations the root-mean-square deviation is also shown. For a low-mass bombardment the r.m.s.

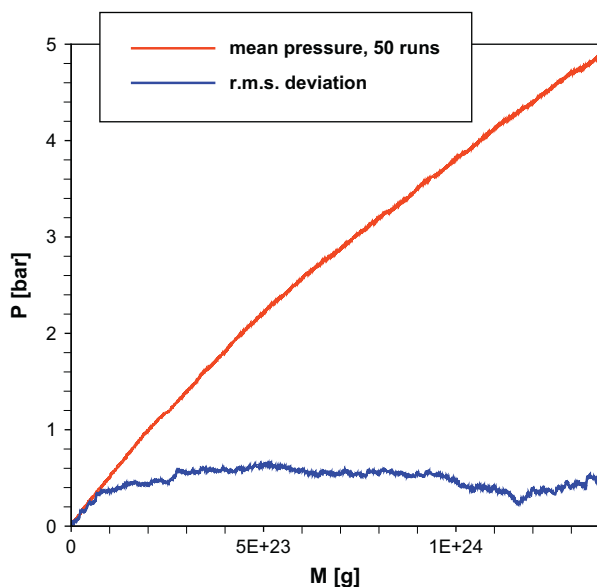


Fig. 12. Martian atmospheric pressure evolution during a heavy bombardment dominated by $x_v = 2\%$ asteroids in dependence on total impactor mass. Mass fraction of volatile-rich ($x_v = 30\%$) KBOs assumed as 1%. Red curve: mean value of 50 runs. Blue: r.m.s. deviation. Initial pressure: 0.01 bar. Total impacting mass is upper limit including martian impact basins according to Frey (2008) and a potential dichotomy-forming event. (For interpretation of the references to color in this figure legend, the reader is referred to the web version of this article.)

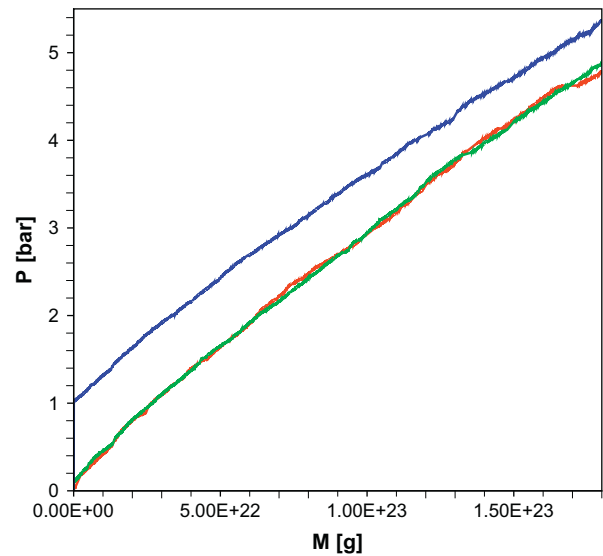


Fig. 13. Effect of variation of initial on final pressure for Mars. To produce a large final pressure only KBOs with high content of atmophiles ($x_v = 30\%$) are considered. All curves are averages resulting from 50 runs.

deviation is rather large. Taking larger samples, that is more runs would have the effect of refining the mean value. The fluctuations are not unexpected because most of the volatiles are delivered in rare events: the impacts of very massive bodies. The actual planetary atmospheres resulting after the highly stochastic heavy bombardment are not described by the mean values, they are single realizations of a stochastic process. A typical mass of 10^{24} g for a dichotomy-causing body is obtained from the impact energy of 10^{29} J, see Nimmo et al. (2008) and the velocity of 14 km s^{-1} preferred by these authors. It is not surprising that a higher content of atmophile molecules leads to a higher atmospheric pressure. The influence of the initial pressure on the final state of the atmosphere is illustrated in Fig. 13 for Mars. It is clearly smaller than statistical effects during the Monte Carlo runs as shown in Fig. 13. A large part of a potentially CO_2 dominated atmosphere could be transformed into carbonates (the total mass of C as CO_2 in sedimentary rock is estimated as 9.1×10^{22} g (Turekian, 2001), or about 17 times the mass of a one bar atmosphere).

5. Discussion and conclusions

The simultaneous consideration of atmospheric loss- and gain processes during an epoch with a strongly enhanced impact rate like it is commonly assumed for the LHB shows that accumulation is the dominant effect. For the parameter set considered the atmospheric pressure is strongly increasing both for Earth and Mars. This result was not expected in this explicitness. The particular profile of a heavy bombardment without a pronounced peak or with multiple peaks in the mass flux would yield similar results. The same should be true in principal if one applies a velocity distribution of the impactors deviating from that resulting in the Nice model we used in our simulations. Actually the Nice model produces even higher losses of atmophile molecules because of the typically larger mean impact velocities as compared with the present.

According to our approach Mars and Earth accumulated atmospheres of one to several bars at the end of the bombardment era largely independent of their initial state. This is in contrast to the results of Pham et al. (2011) who found a net erosion of atmospheres of Mars and Earth during a long-term bombardment by adopting a more efficient atmospheric erosion in terms of a scaled Vickery and Melosh (1990) model. However, if replenishment or

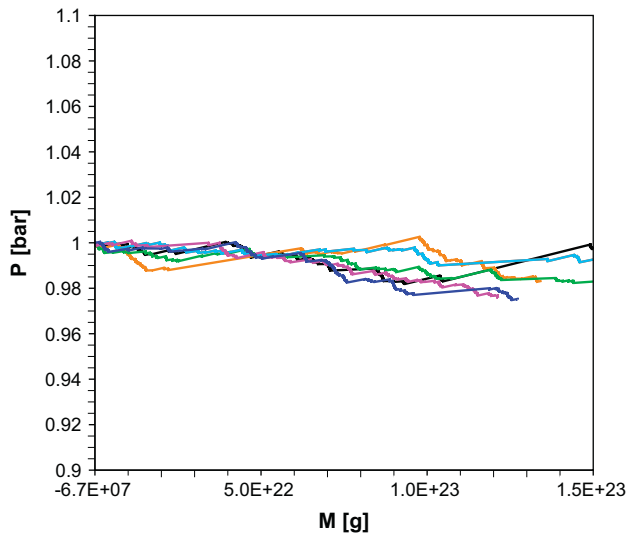


Fig. 14. Special case for Earth where atmospheric erosion is balanced by the feeding process on average. Impactors asteroidal $x_p = 0.2\%$ volatiles. Different curves represent individual Monte Carlo runs.

atmospheric erosion dominates depends on the parametrization used. Meteorite impacts can also cause a more dense atmosphere in this model as stated by Pham et al. (2009), moreover they found that in particular a dense martian atmosphere is not removed by impacts later than the Noachian. Reasons for the different outcome of the models may be the relatively dry composition of the impactors in Pham et al. (2011) and their different assumptions concerning loss of volatiles derived from the impactor and different velocity distributions especially leading to very high impact velocities of the volatile-rich comets. In our model we get a net erosion only for a very dry asteroidal population with a volatile fraction of 0.2% by mass, see Fig. 14, for the velocity distribution and atmospheric conditions of the Earth. This is an unlikely case since meteoritic data suggest a higher average value.

More dense initial atmospheres would further help in slowing down impactors and retaining more of the impact-created vapor plume. The accumulation of an atmosphere is the stronger, the more comets are present in the impactor population, the higher the total mass of impactors is and the more volatiles are existent in the impactors' composition. However, the ratio of the total mass reaching the Earth and Mars during the LHB remains uncertain. Especially Mars may have witnessed considerably more energetic impacts if its crustal dichotomy is of impact origin (Wilhelms and Squyres, 1984; Nimmo et al., 2008; Marinova et al., 2008).

Another result of our calculation is that single impacts of very massive bodies are of more importance for the atmospheric evolution than other input parameters such as the composition of the smaller impactors. A planet can be hit by an impactor of $>10^{22}$ g as has been the case several times for Mars, see Table 4 in Appendix A (several impactors probably had substantially more mass than even a one bar martian or terrestrial atmosphere: $3 - 5 \times 10^{21}$ g). Such an event cannot be predicted with statistical significance, at least for the Earth. If it occurred it had significant consequences. Each such case warrants separate studies using hydrocode simulation and other methods to directly clarify consequences for atmospheres and a possible martian ocean. However the general trend of an increasing atmospheric mass will not change according to semi-analytical models based on highly simplified (Genda and Abe, 2003) or realistic impact simulations (Svetsov, 2005) including an atmosphere, except in the case of singular energetic events with unusually high impact velocity (≥ 30 km s^{-1}).

Table 4

Diameters of cometary or asteroidal bodies forming martian impact basins. Mean density of comets and asteroids assumed as 1000 kg m^{-3} and 2700 kg m^{-3} , target density 3200 kg m^{-3} . Impact velocity 14 km s^{-1} for comets and 11.85 km s^{-1} for asteroids, angle 45° , basin diameters according to Frey (2008).

Impact basin	D (km)	D_p (km) (comet)	D_p (km) (asteroid)
Amenthes	1070	130.8	85.6
Zephyria	1193	147.2	96.3
Daedalia	2639	348.8	228.3
Sirenum	1069	130.7	85.5
SW Daedalia	1278	158.6	103.8
Ares	3300	444.7	291.1
Amazonis	2873	382.6	250.4
In Amazonis	1156	142.3	93.1
Solis	1163	143.2	93.7
N Tharsis	1347	168.0	109.9
Chryse	1725	219.8	143.8
Hematite	1065	130.1	85.2
Scopolus	2250	293.3	192.0
Acidalia	3087	413.6	270.7
North Polar	1600	202.5	132.6
Utopia	3380	456.4	298.8
SE Elysium	1403	175.6	114.9
Hellas	2070	267.9	175.4
Argyre	1315	163.6	107.1
Isidis	1352	168.6	110.4
Σ mass (g)		2.38×10^{23}	1.80×10^{23}

Our model neglects some effects that may be of relevance for atmospheric evolution. We do not consider processes that additionally deliver gases like endogeneous process (e.g. impact-generated volcanism) or the contribution by degassing of target material. On the other hand we disregard hydrodynamic and Jeans escape as further loss mechanisms. However the latter are not specific to the cataclysmic era and would have occurred anyway.

Some assumptions in our simulation method should be discussed in the following. One can find different semi-analytical descriptions in the literature that may lead to somewhat different results for atmospheric erosion. We chose the approach by Svetsov (2000) for reasons discussed in the previous chapter. Despite of widely different physical assumptions models by Genda and Abe (2003) and Svetsov (2007) barely differ in their consequence for large bodies that are the most important ones for the result in this paper. However in an alternative description by Shuvalov (2009) the erosion efficiency decreases very steeply at large sizes, such that above certain size the total escaping atmospheric mass due to large impactors would even be lower than due to a smaller one. This seems to be caused by the grid resolution in the most energetic simulated impacts. Different assumptions and methods can also be found with respect to impactor retention. Some authors state that 50% of a large terrestrial impactor is lost (Jørgensen et al., 2009) if of cometary composition. Others propose a preferential loss of impactor volatiles. In the terrestrial case of a Nice-type LHB even a typical asteroidal impactor could barely avoid almost complete vaporization. There occurs no fast separation of atmospheres and 'rock vapor' when all materials are gaseous and thoroughly mixed. Numerical results (Shuvalov, 2009) demonstrate that most asteroidal and cometary material will be retained at terrestrial impacts for velocities typical during the LHB and support the scaling we applied here. Peculiar impact-produced effects associated with a massive and hot debris cloud are not within the scope of traditional multi-material methods and hydrocodes for elastic-plastic flow. What is not considered using such methods is the effect of mass loading of impact-generated vapor with droplets and particles exerting a drag force additionally slowing down the plume expansion. Simplified to more detailed studies of the effect of atmospheric heating by fast ejecta have been made by Manning

et al. (2009), Artemieva and Ivanov (2004) and Goldin and Melosh (2009), however at much smaller scale of the impact event. The mass of long-range ballistic ejecta may be found in numerical simulations, see for example de Niem et al. (2007b). In the case of the Chicxulub the entire amount of the worldwide impactite layer is about the projectile mass but can hardly be distributed as ballistic ejecta in its entirety (de Niem et al., 2007b). The effect of an ejecta cloud that is partially liquid and more massive than the entire atmosphere would probably be that the atmospheric temperature remains buffered by the melting temperature of silicates irrespective of detailed heating and cooling mechanisms. This temperature alone is insufficient to power hydrodynamic escape. More detailed work is required to understand the role of ejecta for the atmosphere.

An interesting question is how the planets lose their dense atmosphere after the heavy bombardment epoch and evolve into their current state. Several mechanisms like carbonate mineral formation in the oceans followed by subduction, non-thermal ion pickup loss due to solar wind- and X-ray irradiation by the young Sun have been discussed (Zahnle et al., 2007; Kulikov et al., 2007; Lichtenegger et al., 2010; Boeswetter et al., 2010).

Acknowledgements

This research has been supported by the Helmholtz Association through the research alliance “Planetary Evolution and Life”. We thank the unknown reviewers for their constructive comments, which helped in improving the manuscript.

Appendix A

A.1. Genda–Abe model with adiabatic stratification

For an adiabatic density profile $\rho = \rho_0(1 - g_s z(\gamma - 1)/c_0^2)^{1/(\gamma-1)}$, where the gravitational acceleration g_s can be taken as constant (z is restricted to vary in a narrow range such that ρ remains real), $c_0 = (\gamma p_0/\rho_0)^{1/2}$ is the sound speed at the surface. Then the escaping atmospheric mass fraction is given by

$$\left(1 - \frac{\gamma - 1}{c_0^2} g_s z\right)^{\gamma/(\gamma-1)} = \frac{4v(r) - v_{esc}}{3v_{esc}}. \quad (20)$$

This can be inverted for r as function of z . Omitting details, the final expression for the lost mass is Eq. (10) again, with the only substitution $H \rightarrow c_0^2/(g_s \gamma)$. For the same temperature the scale height is identical to that of an isothermal atmosphere.

A.2. Integrals occurring in the models by Svetsov and Vickery and Melosh

The integration in Eq. (2) with the value $k = 5$ preferred by Svetsov (2007) is elementary

$$f(x) = \int_0^x (1 - x^2)^5 dx = x \left(1 - \frac{5}{3}x^2 + 2x^4 - \frac{10}{7}x^6 + \frac{5}{9}x^8 - \frac{1}{11}x^{10}\right), \quad (21)$$

furthermore $f(1) = 256/693$. The integral in Eq. (14) for the impactor loss fraction is of the form

$$I_k := \int_x^1 x^2(1 - x^2)^k dx, \quad (22)$$

where $k = 1/(\gamma - 1)$. For k integer, using partial integration one can show that a recursion relation is valid

$$I_k = \frac{2k}{2k+3} I_{k-1} - \frac{1}{2k+3} x^3(1 - x^2)^k, \quad k > 0, \quad (23)$$

with the initial condition

$$I_0 = \frac{1 - x^3}{3}. \quad (24)$$

For half-integer k the same recursion relation is valid but this time the initial condition is

$$I_{-1/2} = \int_x^1 x^2(1 - x^2)^{-1/2} dx = \frac{1}{2}x(1 - x^2)^{1/2} + \frac{\pi}{4} - \frac{1}{2} \arcsin x. \quad (25)$$

A.3. Martian heavy bombardment

Diameters and the mass of bodies forming the largest martian impact basins have been estimated, using the data of Frey (2008) and the scaling law by Schmidt and Housen (1987) for solid rock as target material combined with a relation due to Croft (1982) relating transient cavity diameters to final diameters. The dataset contains many so-called quasi-circular depressions and so is not unequivocal (Werner, 2008). Table 4 shows the resulting impactor diameters assuming an average impact velocity of 14 km s^{-1} for KBOs (Levison et al., 2001). A value of 11.85 km s^{-1} is chosen for main-belt asteroids that corresponds to the mean value in simulations for the Nice model for these bodies. An average impact angle of 45° is taken into account by modifying the transient cavity volume in a way suggested by Pierazzo and Melosh (2000). The average impact velocity is not necessarily typical for the largest impact basins because these are low-probability events and exceptionally high-velocity impactors with only moderate size may contribute disproportionately. The impacting mass if exclusively due to comets would be $2.38 \times 10^{23} \text{ g}$, and if due to asteroids $1.80 \times 10^{23} \text{ g}$, both numbers being lower limits because they neglect the considerable amount of mass in smaller bodies. Circumstantially these numbers are close to those found for the Earth, corresponding to a lunar LHB including all Nectarian-age basins, see Ryder (2002), and also South-Pole Aitken. This comparison does not regard a potential martian crustal dichotomy-forming body that would add about 10^{24} g alone and rise the mass flux ratio by another order of magnitude. This follows from the required kinetic energy of about 10^{29} J (Wilhelms and Squyres, 1984; Nimmo et al., 2008; Marinova et al., 2008). Omitting South-Pole Aitken from the lunar set has a similar effect on this ratio. This shows that even without a hypothetical Borealis basin Mars suffered dramatically more massive and energetic impacts per unit area than the Earth and thus has a considerably different cratering chronology, even if neglecting some of the quasi-circular depressions included by Frey (2008) from Table 4.

References

- Abe, Y., Matsui, T., 1985. The formation of an impact-generated H_2O atmosphere and its implications for the early thermal history of the Earth. *J. Geophys. Res.* 90 (Suppl.), C545–C559.
- Ahrens, T.J., 1993. Impact erosion of terrestrial planetary atmospheres. *Annu. Rev. Earth Planet. Sci.* 21, 525–555.
- Altwegg, K., Balsiger, H., Geiss, J., 1999. Composition of the volatile material in Halley's coma from in situ measurements. In: Altwegg, K., Ehrenfreund, P., Geiss, J., Huebner, W. (Eds.), *Composition and Origin of Cometary Materials*. Kluwer Academic Publishers, pp. 3–18.
- Artemieva, N.A., Ivanov, B.A., 2004. Launch of martian meteorites in oblique impacts. *Icarus* 171, 84–101.
- Boeswetter, A., Lammer, H., Kulikov, Y., Motschmann, U., Simon, S., 2010. Non-thermal water loss on the early Mars: 3D multi-ion hybrid simulations. *Planet. Space Sci.* 58, 2031–2043.
- Bottke, W.F., Durda, D.D., Nesvorný, D., Jedicke, R., Morbidelli, A., Vokrouhlický, D., Levison, H., 2005. The fossilized size distribution of the main asteroid belt. *Icarus* 175, 111–140.
- Bottke, W.F., Levison, H.F., Nesvorný, D., Dones, L., 2007. Can planetesimals left over from terrestrial planet formation produce the lunar late heavy bombardment. *Icarus* 190, 203–223.

- Chen, G.Q., Ahrens, T.J., 1997. Erosion of terrestrial plane atmosphere by surface motion after a large impact. *Phys. Earth Planet. Interiors* 100, 21–26.
- Croft, S.K., 1982. The scaling of complex craters. *J. Geophys. Res.* 90 (Suppl.), C828–C842.
- Ćuk, M., Gladman, B.J., 2009. The fate of primordial lunar Trojans. *Icarus* 199, 237–244.
- Dauphas, N., 2003. The dual origin of the terrestrial atmosphere. *Icarus* 165, 326–339.
- de Niem, D., Kührt, E., Motschmann, U., 2007b. Ejecta range: A simulation study of terrestrial impacts. *Planet. Space Sci.* 55, 900–914.
- Frey, H., 2008. Ages of very large impact basins on Mars: Implications for the heavy bombardment in the inner Solar System. *Geophys. Res. Lett.* 35, L13203. <http://dx.doi.org/10.1029/2008GL03515>.
- Genda, H., Abe, Y., 2003. Survival of a proto-atmosphere through the state of giant impacts: The mechanical aspects. *Icarus* 164, 149–162.
- Goldin, T.J., Melosh, H.J., 2009. Self-shielding of thermal radiation by Chicxulub ejecta: Firestorm or fizzle? *Geology* 37, 1135–1138.
- Gomes, R., Levison, H.F., Tsiganis, K., Morbidelli, A., 2005. Origin of the cataclysmic late heavy bombardment period of the terrestrial planets. *Nature* 43, 466–469.
- Grady, M., Wright, I.P., 2003. Elemental and isotopic abundances of carbon and nitrogen in meteorites. *Space Sci. Rev.* 106, 231–248.
- Grott, M., Morschhauser, A., Breuer, D., Hauber, E., 2011. Volcanic outgassing of CO₂ and H₂O on Mars. *Earth Planet. Sci. Lett.* 308, 391–400.
- Hamano, K., Abe, Y., 2006. Impact erosion of atmospheres: Substantial atmospheric loss by impact-induced vaporexpansion. In: *Workshop on the Role of Volatiles and Atmospheres on Martian Craters*, Lunar and Planetary Institute, Houston (abstract 3031).
- Hartogh, P. et al., 2011. Ocean-like water in the Jupiter-family comet 103P/Hartley 2. *Nature* 478, 218–220. <http://dx.doi.org/10.1038/nature10519>.
- Hills, J.G., Goda, M.P., 1993. The fragmentation of small asteroids in the atmosphere. *Astron. J.* 105, 1114–1144.
- Holsapple, K.A., Schmidt, R.M., 1987. Point source solutions and coupling parameters in cratering mechanics. *J. Geophys. Res.* 92, 6350–6376.
- Housen, K.R., Holsapple, K.A., 2011. Ejecta from impact craters. *Icarus* 211, 856–875.
- Ivanov, B.A., 2001. Mars/Moon cratering rate estimates. *Space Sci. Rev.* 96, 87–104.
- Jørgensen, U.G., Appel, P.W.U., Hatsukawa, Y., Frei, R., Toh, Y., Oshima, M., 2009. The Earth–Moon system during the late heavy bombardment period – Geochemical support for impacts dominated by comets. *Icarus* 204, 368–380.
- Koerber, C., 2003. The late heavy bombardment in the inner Solar System: Is there any connection to Kuiper belt objects? *Earth Moon Planets* 92, 79–87.
- Korycansky, D.G., 1992. An off-center explosion in a radially stratified medium: Kompaneets approximation. *Astrophys. J.* 398, 184–189.
- Kulikov, Y.N. et al., 2007. A comparative study of the influence of the active young Sun on the early atmospheres of Earth, Venus, and Mars. *Space Sci. Rev.* 129, 207–243.
- Levison, H.F., Dones, L., Chapman, C.R., Stern, S.A., Duncan, M.J., Zahnle, K., 2001. Could the lunar “late heavy bombardment” have been triggered by the formation of Uranus and Neptune. *Icarus* 151, 286–306.
- Lichtenegger, H.I.M., Lammer, H., Grießmeier, J.-M., Kulikov, Yu. N., von Paris, P., Hausleitner, W., 2010. Aeronomical evidence for higher CO₂ levels during Earth’ Hadean epoch. *Icarus* 210, 1–7.
- Manning, C.V., Zahnle, K.J., McKay, C.P., 2009. Impact processing of nitrogen on early Mars. *Icarus* 199, 273–285.
- Marinova, M.M., Aharonson, O., Asphaug, E., 2008. Mega-impact formation of the Mars hemispheric dichotomy. *Nature* 453, 1216–1219. <http://dx.doi.org/10.1038/nature07070>.
- Marty, B., Meibom, A., 2007. Noble gas signature of the late heavy bombardment on the Earth’s atmosphere. *eEarth* 2, 43–49.
- Matsumoto, M., Nishimura, T., 1998. Mersenne Twister: A 623-dimensionally equidistributed uniform pseudorandom number generator. *ACM Trans. Model. Comput. Simul.* 8, 3–30.
- Melosh, H.J., 1989. *Impact Cratering: A Geologic Process*. Oxford University Press/Clarendon Press, New York/Oxford, 245pp.
- Melosh, H.J., Vickery, A.M., 1989. Impact erosion of the primordial atmosphere of Mars. *Nature* 338, 487–489.
- Morbidelli, A., Levison, H.F., Bottke, W.G., Dones, L., Nesvorný, D., 2009. Considerations on the magnitude distributions of the Kuiper belt and the Jupiter Trojans. *Icarus* 202, 310–315.
- Morbidelli, A., Brasser, R., Gomes, R., Levison, H.F., Tsiganis, K., 2010. Evidence from the asteroid belt for a violent past evolution of Jupiter’s orbit. *Astron. J.* 140, 1391–1401.
- Newman, W.I., Symbalisty, E.M.D., Ahrens, T.J., Jones, E.M., 1999. Impact erosion of planetary atmospheres: Some surprising results. *Icarus* 138, 224–240.
- Nimmo, F., Hart, S.D., Korycansky, D.G., Agnor, C.B., 2008. Implications of an impact origin for the martian hemispheric dichotomy. *Nature* 453, 1220–1224. <http://dx.doi.org/10.1038/nature07025>.
- Nishimura, T., 2000. Tables of 64-bit Mersenne Twisters. *ACM Trans. Model. Comput. Simul.* 10, 348–357.
- Pham, L.B.S., Karatekin, Ö., Dehant, V., 2009. Effects of meteorite impacts on the atmospheric evolution of Mars. *Astrobiology* 9 (1), 45–54.
- Pham, L.B.S., Karatekin, Ö., Dehant, V., 2011. Effects of impacts on the atmospheric evolution: Comparison between Mars, Earth, and Venus. *Planet. Space Sci.* 59, 1087–1092.
- Pierazzo, E., Melosh, H.J., 2000. Melt production in oblique impacts. *Icarus* 145, 252–261.
- Ryder, G., 2002. Mass flux in the ancient Earth–Moon system and benign implications for the origin of life on Earth. *J. Geophys. Res.* 107 (E4), 1–13 (Cite id: 5022).
- Sanzovo, G.C., Trevisan Sanzovo, D., de Almeida, A.A., 2009. On the relationship between gas and dust in 15 comets: An application Comet 103P/Hartley 2 target of the NASA EPOXI mission of opportunity. *Proc. IAU Symp.* 263, 272–276.
- Schaefer, L., Fegley Jr., B., 2010. Chemistry of atmospheres formed during accretion of the Earth and other terrestrial planets. *Icarus* 208, 438–448.
- Schmidt, R.M., Housen, K.R., 1987. Some recent advances in the scaling of impact and explosion cratering. *Int. J. Impact Eng.* 5, 543–560.
- Senshu, H., Kuramoto, K., Matsui, T., 2002. Thermal evolution of a growing Mars. *J. Geophys. Res.* 107 (E12), 5118.
- Shuvalov, V.V., 1999. Multi-dimensional hydrodynamic code SOVA for interfacial flows: Application to the thermal layer effect. *Shock Waves* 9, 381–390.
- Shuvalov, V.V., 2009. Atmospheric erosion induced by oblique impacts. *Meteorit. Planet. Sci.* 44 (8), 1095–1105.
- Shuvalov, V.V., 2010. Atmospheric erosion induced by oblique impacts. *Lunar Planet. Sci.* 41, Abstract No 1191.
- Sleep, N.H., Zahnle, K.J., Kasting, J.F., Morowitz, H.J., 1989. Annihilation of ecosystems by large asteroid impacts on the early Earth. *Nature* 342, 139–142.
- Stuart, J.S., Binzel, R.P., 2004. Bias-corrected population, size distribution, and impact hazard for the near-Earth objects. *Icarus* 170, 295–311.
- Svetsov, V.V., 2000. On the efficiency of the impact mechanism of atmospheric erosion. *Solar Syst. Res.* 34 (5), 398–410.
- Svetsov, V.V., 2003. Numerical modeling of large asteroidal impacts on the Earth. *Int. J. Impact Eng.* 29, 671–682.
- Svetsov, V.V., 2005. Numerical simulations of very large impacts on the Earth. *Planet. Space Sci.* 53, 1205–1220.
- Svetsov, V.V., 2007. Atmospheric erosion and replenishment induced by impacts of cosmic bodies upon the Earth and Mars. *Solar Syst. Res.* 41 (1), 28–41.
- Tonks, W.B., Melosh, H.J., 1992. Core formation by giant impacts. *Icarus* 100, 326–346.
- Turekian, K.K., 2001. Origin of the oceans. In: Steele, J.H., Thorpe, S.A., Turekian, K.K. (Eds.), *Encyclopedia of Ocean Sciences*, vol. 2, pp. 2055–2058.
- Vickery, A.M., Melosh, H.J., 1990. Atmospheric erosion and impactor retention in large impacts. With application to mass extinctions. *Geol. Soc. Am. Spec. Pap.* 247, 289–300.
- Walker, J.C.G., 1986. Impact erosion of planetary atmospheres. *Icarus* 68, 87–98.
- Werner, S.C., 2008. The early martian evolution – Constraints from basin formation ages. *Icarus* 195, 45–60.
- Wetherill, G.W., 1975. Late heavy bombardment of the Moon and terrestrial planets. *Proc. Lunar Sci. Conf.* 6, 1539–1561.
- Wilhelms, D.E., Squyres, S.W., 1984. The martian hemispheric dichotomy may be due to a giant impact. *Nature* 309, 138–140.
- Zahnle, K.J., 1990. Atmospheric chemistry by large impacts. *Geol. Soc. Am. Spec. Pap.* 247, 271–288.
- Zahnle, K. et al., 2007. Emergence of a habitable planet. *Space Sci. Rev.* 129, 35–78.
- Zahnle, K.J., Sleep, N.H., 1997. Impacts and the early evolution of life. In: Thomas, P.J., Chyba, C.F., McKay, C.P. (Eds.), *Comets and the Origin and Evolution of Life*. Springer-Verlag, New York, pp. 175–208.
- Zahnle, K.J., Kasting, J.F., Pollack, J.B., 1988. Evolution of a steam atmosphere during Earth’ accretion. *Icarus* 74, 62–97.
- Zahnle, K., Pollack, J.B., Grinspoon, D., 1992. Impact-generated atmospheres over Titan, Ganymede, and Callisto. *Icarus* 95, 1–23.
- Zeldovich, Ya.B., Raizer, Yu.P., 1967. *Physics of Shock Waves and High-Temperature Hydrodynamic Phenomena*. Academic Press, New York, San Francisco, London.